Generation and Propagation of Downwelling Fronts

T. J. SIMONS

Canada Centre for Inland Waters, Burlington, Ontario, Canada L7R 4A6

(Manuscript received 24 October 1977, in final form 6 February 1978)

ABSTRACT

The dynamics of downwelling fronts observed along the steep and elongated southern shore of Lake Ontario are investigated by considering the nonlinear response to surface forcing of one-layer and two-layer fluids on a rotating, semi-infinite plane. Analytical and numerical solutions for idealized situations exhibit typical characteristics of the observed fronts such as offshore propagation and periodic recurrence with near-inertial periods. A numerical simulation of an actual downwelling episode in Lake Ontario shows that this type of model reproduces the observed behavior of the thermocline as well as the associated oscillatory currents. It is concluded that the fronts are to be visualized as internal surges associated with the oscillatory rather than the quasi-geostrophic response of a lake to wind.

1. Introduction

Surfaces of apparent density discontinuity occur in nature in many different forms and the governing dynamics vary greatly as a function of time and space scales involved. Large-scale oceanic fronts resemble their atmospheric counterparts and this analogy may be useful to explore the associated water circulation (Rao and Murty, 1973). An interesting example is the quasi-permanent frontal zone off the Oregon Coast during the upwelling season (Mooers *et al.*, 1976), which is intimately connected with baroclinic alongshore currents. By contrast, there are small-scale frontal zones such as the boundaries of river plumes in salt water bodies (Garvine and Monk, 1974) and the quasi-discontinuous temperature distributions associated with the steepening of internal waves in a stratified fluid. The latter have an hydraulic analogy in the form of an internal surge in a two-layer system where the effects of rotation are negligible. Internal bores have been observed, for example, in long narrow lakes (Thorpe, 1971; Hunkins and Fliegel, 1973), in coastal waters (Winant, 1974), and at the interface between Atlantic and Mediterranean water in the Straits of Gibraltar (Boyce, 1975).

Recently, temperature distributions with frontal characteristics, but somewhat peculiar dynamics, have been observed by high-resolution measurements in Lake Ontario (Boyce and Mortimer, 1978). These temperature fronts were generated by strong downwelling along the steep, elongated southern shore of the Lake and were seen to persist over at least a few inertial periods. The initial downwelling was caused by the passage of a brief but intense westerly wind impulse. Following the storm, a steep thermal front was found to separate warm near-shore water from cooler water in the open lake. The front displayed distinct near-inertial properties such as periodic offshore progressions accompanied by surge-like features. Simultaneous observations for three north-south cross-sections of Lake Ontario indicated that this phenomenon extended along the whole south shore, suggesting that its dynamics are essentially independent of the alongshore coordinate.

As discussed by Mortimer (1977), the fronts appear to belong to the class of internal surges, but the near-inertial periodicities in their behavior and the simultaneous presence of quasi-geostrophic coastal jets suggest that the earth's rotation must play an important role in their dynamics. At times they do indeed appear as intensifications and slight lateral displacements of the downward sloping thermocline which is presumably in approximate balance with vertical shears of alongshore currents. The purpose of this study is to evaluate the relationships between such downwelling fronts and the oscillatory and the quasi-geostrophic response of near-shore waters to wind forcing.

2. The model

The dynamics of the system will be investigated by starting from the model used in Cahn's (1945) study of the geostrophic adjustment problem and then extending the solutions to a two-layer system. In particular, the analysis will recall recent applications of this model by Houghton (1969) and Crepon (1967) dealing with nonlinear effects and the near-shore response to wind forcing, respectively. The model consists of a hydrostatic and homogene-

0022-3670/78/0571-0581$05.50

ous layer of fluid with a free upper boundary and a flat bottom in a rotating coordinate system, but the solutions are assumed to be independent of one of the horizontal coordinates. The equations are conveniently written in nondimensional form by defining

$$\left.\begin{aligned} &t \doteq ft', \quad x = x'/R, \quad h = h'/H \\ &(u,v) = (u',v')/C, \quad (\tau_x,\tau_y) = (\tau'_x,\tau'_y)/\rho fHC \end{aligned}\right\}, \tag{1}$$

where the primes denote the original dimensional variables and t is time, x the space coordinate along which the solutions are allowed to vary, h the thickness of the fluid layer, u and v are the components of the vertically averaged velocity along the x coordinate and normal to it, respectively, τ_x and τ_y are the corresponding components of the surface stress, f is the Coriolis parameter, H a reference depth, $C \equiv (gH)^{1/2}$ the corresponding wave speed, $R \equiv C/f$ the Rossby radius of deformation and ρ water density. With the usual approximation for the nonlinear terms, the vertically averaged equations of motion and the continuity equation may be written

$$\left.\begin{aligned} &\frac{\partial u}{\partial t} - v + u\frac{\partial u}{\partial x} + \frac{\partial h}{\partial x} = \frac{\tau_x}{h} \\ &\frac{\partial v}{\partial t} + u + u\frac{\partial v}{\partial x} = \frac{\tau_y}{h} \\ &\frac{\partial h}{\partial t} + \frac{\partial}{\partial x}(hu) = 0 \end{aligned}\right\}. \tag{2}$$

The above one-layer model is a convenient tool for an analysis of the behavior of a stratified lake which may be represented by a two-layer system. A discussion of this generalization of the one-layer results will be presented, but for the moment it is sufficient to realize that the above equations describe the dynamics of the upper layer of a two-layer system when the second layer is much deeper than the first and the wave-speed C is replaced by the corresponding internal phase speed. In particular, then, a positive change of depth h can be identified with a downward displacement of the thermocline in a stratified body of water.

In the following, some of the solutions to the above equations and the corresponding two-layer system will be obtained by numerical integration. In all these cases use is made of a two-step version of the method proposed by Lax and Wendroff (1960), which is known to be suitable for the present kind of problem. The scheme damps higher wavenumbers and hence the oscillations which tend to form in the vicinity of a front are suppressed. As a result, the total energy of the model will decrease noticeably when the slope of a wave front becomes vertical to form a hydraulic "jump". The validity of numerical integration beyond this point may be in doubt because of this artificial smoothing and also because the hydrostatic assumption can no longer be justified. The subsequent comparison with observations, however, indicates that the primary physical processes are probably represented in an acceptable manner.

Since it is desirable to conserve both mass and momentum in the numerical computations, the system of equations is written in terms of the transport components $(U,V) \equiv (hu,hv)$ as

$$\left.\begin{aligned} &\frac{\partial U}{\partial t} - V + \frac{\partial}{\partial x}\left(\frac{U^2}{h} + \frac{h^2}{2}\right) = \tau_x \\ &\frac{\partial V}{\partial t} + U + \frac{\partial}{\partial x}\left(\frac{UV}{h}\right) = \tau_y \\ &\frac{\partial h}{\partial t} + \frac{\partial U}{\partial x} = 0 \end{aligned}\right\}. \tag{3}$$

The numerical integration over one time increment Δt consists of the following two steps. First, tentative values of all variables are predicted at time level $t + \frac{1}{2}\Delta t$ for locations centered between two grid points. In this step the initial values at time t and the Coriolis terms are averaged over two adjacent mesh points and the space derivatives are approximated by centered differences. Next, new values at time $t + \Delta t$ are predicted at the grid points by stepping forward from the original time level t and using the tentative values at $t + \frac{1}{2}\Delta t$ to evaluate the Coriolis terms and the space derivatives. Stability is insured if the space increment Δx is greater than the maximum value of $\Delta t(u + h^{1/2})$, in nondimensional variables.

3. Nonlinear effects

The nonlinear aspects of the above system of equations may be conveniently illustrated by recalling Houghton's (1969) treatment of the problem in the absence of wind forcing. Consider, then, a simple gravity wave, initially containing no v component of fluid velocity and propagating into an environment which is at rest relative to the rotating frame of reference. In terms of the nondimensional variables (1) the initial conditions are

$$\left.\begin{aligned} &u = \begin{cases} \alpha(1 - |x|/\beta), & |x| \leq \beta \\ 0, & |x| > \beta \end{cases} \\ &v = 0, \quad h = \left(1 + \frac{u}{2}\right)^2, \quad \text{all } x \end{aligned}\right\}. \tag{4}$$

Clearly, α represents the initial Froude number at the crest of the wave, while β is the ratio of the initial wavelength to the radius of deformation. In the absence of rotation, this type of wave will form

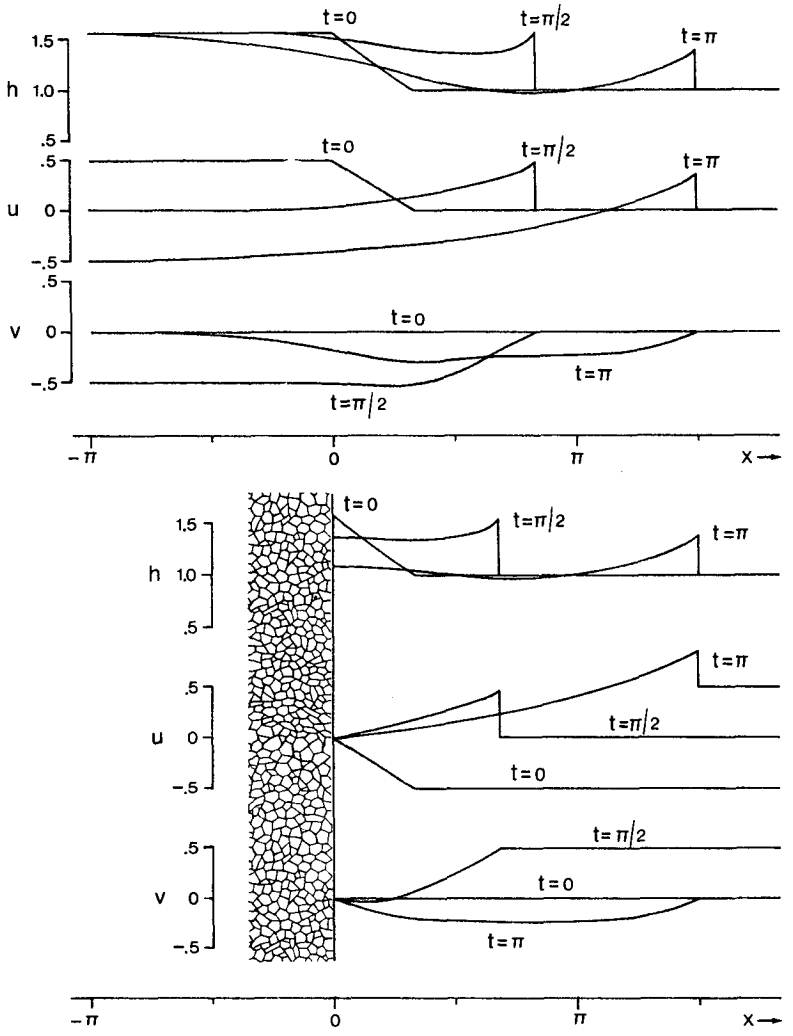

FIG. 1. Time and space variations of surface elevation and fluid velocity for a simple gravity wave on a rotating infinite plane (top) and on a half-plane bounded by a solid wall (bottom). All variables are nondimensionalized according to Eq. (1).

a jump because the slope of the characteristics is equal to $u + h^{1/2}$, and the crest of the wave will tend to overtake the leading edge. The purpose of Houghton's study was to determine to what extent jump formation is opposed by the dispersion due to the earth's rotation. The analysis was carried out for $0 < \alpha < 0.5$ and $0 < \beta < 1$, and showed that delay of jump formation and reduction of jump amplitude were proportional to increasing β and decreasing α, i.e., increasing effects of rotation and decreasing nonlinear effects, respectively.

By recourse to the linear solution for the wind-forced downwelling problem to be discussed next, an appropriate length scale may be taken to be $\beta = 1$, while the value of α will be determined by the wind stress at the surface and the resulting inertial motion away from the shore. For a typical value of $\alpha = 0.5$, the formation of a jump would be delayed by about 0.2 nondimensional time units, while the amplitude would be reduced by not more than 20% according to Houghton's (1969) Figs. 4–5. To illustrate the solution for these parameter values, the upper part of Fig. 1 shows the configuration of this type of wave as a function of nondimensional time and space. It will be noted that the initial conditions differ from Eq. (4) behind the wave crest, but this does not affect the leading side of the wave. The solution was obtained by the aforementioned Lax-Wendroff scheme with a spatial resolution of $\Delta x = 0.015$, which is essentially equivalent to Houghton's numerical method.

The above results can be interpreted in terms of the present problem by the following argument. Behind the wave crest in the upper part of Fig. 1,

inertial motion develops as a result of the Coriolis force. We now impose an initial velocity $u = -\alpha$ on the whole system. In the absence of rotation, this would be equivalent to a steady translation of the coordinate system, but in the present case, the result will be an inertial motion ahead of the wave. To the left of the initial position of the wave crest the effects are in first approximation the same as in the absence of rotation, in which case the fluid would be at rest behind this wave. Thus the solution for positive x is only weakly affected by a solid boundary at $x = 0$, as demonstrated at the bottom of Fig. 1. It may be noted that the initial superposition of the negative u component leads not only to inertial-type fluid motion ahead of the wave but also to a nonsteady wave speed. Thus, the wave slows down when it moves against the current ($0 < t < \pi/2$) and it speeds up when it moves with the flow ($\pi/2 < t < \pi$).

4. Wind forcing

Before turning to the complete nonlinear problem of wind-induced motions near a shore, it is useful to consider the salient features of corresponding linear solutions. The linearized version of the system of nondimensional equations (3) reads

$$\frac{\partial U}{\partial t} - V + \frac{\partial h}{\partial x} = \tau_x, \quad \frac{\partial V}{\partial t} + U = \tau_y,$$
$$\frac{\partial h}{\partial t} + \frac{\partial U}{\partial x} = 0, \tag{5}$$

with initial conditions $U = 0$, $V = 0$, $h = 1$, and boundary conditions $U = 0$ at the wall ($x = 0$) and U, V, h finite for $x \to \infty$. The solutions are conveniently obtained by separating the two cases $\tau_x = 0$, $\tau_y \neq 0$ (alongshore wind) and $\tau_y = 0$, $\tau_x \neq 0$ (wind normal to shore), and by eliminating h and V in the first case and h and U in the second. The respective equations are

$$\left.\begin{aligned} \frac{\partial^2 U}{\partial t^2} - \frac{\partial^2 U}{\partial x^2} + U &= \tau_y \\ \frac{\partial^2 V}{\partial t^2} - \frac{\partial^2 V}{\partial x^2} + V &= -\tau_x \end{aligned}\right\}, \tag{6}$$

where the boundary condition at the wall for the second equation is $V = 0$, owing to the original boundary condition and the second of Eqs. (5).

Consider the response to a wind suddenly applied at $t = 0$ and remaining constant afterward. This is a special case of the problem solved by Crepon (1967) in the form of convolution integrals and Bessel functions, by employing the method of Laplace transforms. A simple and illuminating solution for the present case may be obtained by realizing that the solution should be the sum of the solution to the time-independent forced equation plus a solution to the homogeneous equation which cancels the former at the initial time. The same argument was employed by Csanady (1973) to illustrate the corresponding channel problem. The appropriate forced solutions to (6) are clearly given by $U = \tau_y[1 - \exp(-x)]$ and $V = -\tau_x[1 - \exp(-x)]$ for the two wind directions, respectively, with the corresponding solutions for the remaining variables determined from (5). The free oscillations are combinations of trigonometric functions with argument $(kx - \sigma t)$, where $\sigma^2 = 1 + k^2$ and k is the wavenumber, such that the initial conditions and the boundary conditions are satisfied. By recalling the Fourier integral representations

$$\frac{2}{\pi}\int_0^\infty \frac{k \sin kx}{1 + k^2}\,dk = e^{-x}, \quad \frac{2}{\pi}\int_0^\infty \frac{\cos kx}{1 + k^2}\,dk = e^{-x},$$
$$\frac{2}{\pi}\int_0^\infty \frac{\sin kx}{k}\,dk = 1,$$

(see, e.g., Carslaw, 1930, Chap. 10) it can be readily verified that the desired solutions are

$$\left.\begin{aligned} U/\tau_y &= 1 - e^{-x} \\ &\quad - \frac{2}{\pi}\int_0^\infty k^{-1}\sigma^{-2} \sin kx \cos\sigma t\,dk \\ V/\tau_y &= te^{-x} + \frac{2}{\pi}\int_0^\infty k^{-1}\sigma^{-3} \sin kx \sin\sigma t\,dk \\ \delta h/\tau_y &= -te^{-x} + \frac{2}{\pi}\int_0^\infty \sigma^{-3} \cos kx \sin\sigma t\,dk \end{aligned}\right\} \tau_x = 0,$$
$$\left.\begin{aligned} U/\tau_x &= \frac{2}{\pi}\int_0^\infty k^{-1}\sigma^{-1} \sin kx \sin\sigma t\,dk \\ V/\tau_x &= e^{-x} - 1 \\ &\quad + \frac{2}{\pi}\int_0^\infty k^{-1}\sigma^{-2} \sin kx \cos\sigma t\,dk \\ \delta h/\tau_x &= -e^{-x} + \frac{2}{\pi}\int_0^\infty \sigma^{-2} \cos kx \cos\sigma t\,dk \end{aligned}\right\} \tau_y = 0, \tag{7}$$

where $\delta h \equiv h - 1$. It is seen that the contributions from the higher wavenumbers decrease in proportion to some power of σ and the oscillatory solutions will exhibit periodicities which tend to, but never attain, the inertial period. Another property of the solutions, which is more apparent from Cahn's (1945) and Crepon's (1967) presentations in terms of Bessel functions, is that the leading edge of the perturbation moves away from the wall with the shallow water wave speed C.

For practical applications, it is of interest to consider a suddenly imposed wind of finite duration.

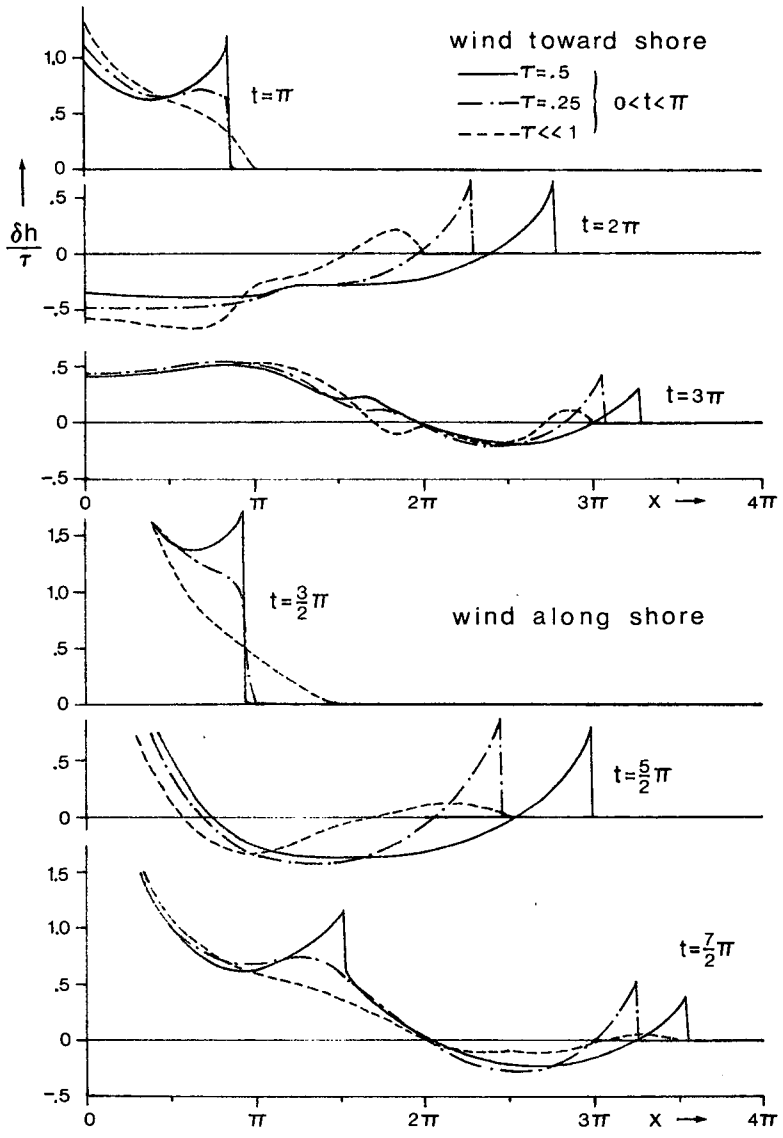

FIG. 2. Linear and nonlinear solutions for surface variations caused by a wind impulse toward the shore (top) and a wind impulse alongshore with the shore on the right (bottom).

The solution follows from (7) by superposition of the solution for a negative wind impulse with a suitable shift in time. It is seen from (7) that the oscillatory component, for a given wind speed, will be greatest if the nondimensional wind duration approximates an odd multiple of π. The surface variations caused by this type of forcing are illustrated by the dashed curves of Fig. 2 for winds blowing toward the shore and along the shore (with the shore on the right), respectively. The times selected are those for which the shoreward component of the inertial motion in open water is zero and hence the oscillatory surface deflections tend to approach their extreme values. For comparison of the convergence of various solution methods, the linear solutions were also computed from Crepon's (1967) integrals and by the numerical integration procedure used for the nonlinear problem.

The nonlinear effects will depend on the magnitude and the duration of the forcing and the solutions cannot be presented with the same generality. With a view to the strongly periodic character of the observations to be discussed, the present experiments will concentrate on a wind impulse of duration π. With regard to the relation between nonlinear effects and the magnitude of the stress, it is useful to consider the wind-induced motion away from the shore. In open water the above wind impulse will cause a pure inertial

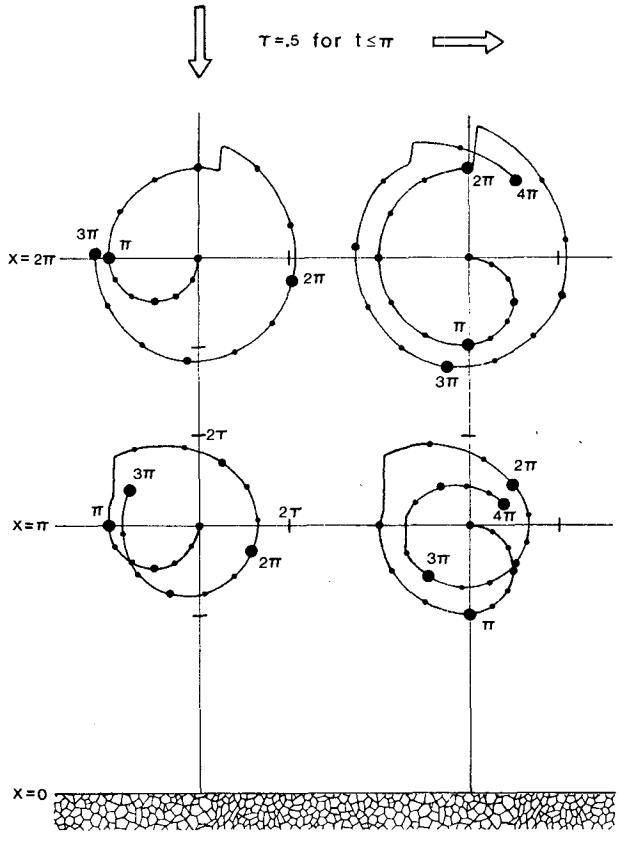

FIG. 3. Hodographs of currents in a nonlinear model for a wind impulse toward the shore (left) and parallel to the shore (right).

motion with nondimensional amplitude 2τ, which may be compared with the Froude number α in (4). This relationship allows for a direct comparison with the wave problem illustrated in Fig. 1.

Fig. 2 presents nonlinear solutions for the surface elevations as a function of time, distance from shore and wind stress, all in nondimensional form as defined by (1). Typical hodographs of the computed currents are shown in Fig. 3. It will be seen that, starting from $t = \pi$ for the case of a wind blowing toward the shore, and from $t = 3\pi/2$ for wind along the shore, the solutions are comparable to the lower part of Fig. 1 after $t = \pi/2$. At these times the oscillatory surface deflections reach large positive values, while the inertial current is aligned with the shore. It is also seen that a secondary front may form during the next cycle of the surface oscillation, similar to the observations considered in this study. In the hodographs of Fig. 3, the signature of the front appears as a sudden increase in the current component away from the shore, which also may be seen from Fig. 1.

It was noted before that the wave front cannot propagate with a uniform velocity due to the rotating fluid motion ahead of the wave. This effect is illustrated in Fig. 4, which shows the positions of the fronts as a function of time and nonlinear effects depending on wind stress. The black circles indicate the times for which the solutions were shown in Fig. 2. There are two effects causing changes in propagation speed of the wave. The first one is a net increase in wave displacement over a complete inertial period (time interval 2π), as expected from nonlinear solutions without rotation. The second effect is a periodic variation of propagation speed superimposed on the former. This effect could be incorporated in the linear solutions by including a linearized advection term with the shoreward component of the inertial motion acting as the advecting velocity.

5. Two-layer system

We next consider a stratified fluid with a rigid upper surface but the depth a function of distance from the shore. The stratification is assumed to be concentrated at a single interface and the hydrostatic and the Boussinesq approximations are employed. The equations for each layer are then of the same general form as those for the single-layer model. For easy comparison with the foregoing, it is convenient to express the mass transport in the lower layer in terms of the transport in the upper layer and the total transport, and to eliminate the surface pressure gradients by subtracting the equations for the two layers. If again the solutions are taken to be independent of y, then the total mass transport normal to the shore must vanish by virtue of the continuity equation and the boundary condi-

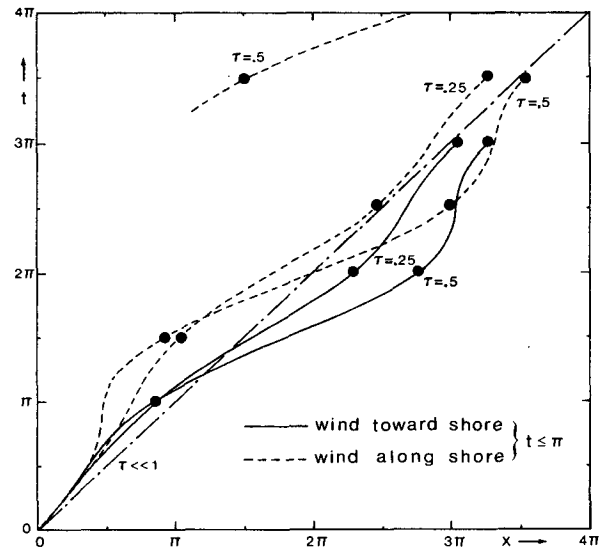

FIG. 4. Position of wave fronts of Fig. 2 as a function of time. Black circles indicate times for which solutions are shown in Fig. 2.

tion at the shore, and the equations become

$$\left.\begin{aligned}
&\frac{\partial U}{\partial t} - fV + \frac{D-h}{D}\left[\frac{\partial}{\partial x}\left(\frac{U^2}{h} + \frac{g\epsilon h^2}{2}\right) - \frac{\tau_x}{\rho}\right] \\
&\qquad - \frac{h}{D}\left[\frac{\partial}{\partial x}\left(\frac{U^2}{D-h}\right) - fM\right] = 0 \\
&\frac{\partial V}{\partial t} + fU + \frac{D-h}{D}\left[\frac{\partial}{\partial x}\left(\frac{UV}{h}\right) - \frac{\tau_y}{\rho}\right] \\
&\qquad - \frac{h}{D}\left[\frac{\partial}{\partial x}\left(\frac{UV - UM}{D-h}\right) + \frac{\partial M}{\partial t}\right] = 0 \\
&\frac{\partial h}{\partial t} + \frac{\partial U}{\partial x} = 0
\end{aligned}\right\}, \quad (8)$$

where $(U,V) \equiv (hu,hv)$ is the mass transport in the upper layer, h the upper layer depth, $D(x)$ the total water depth, M the component of the total mass transport along the shore, $\epsilon \equiv \Delta\rho/\rho$ the density difference across the interface, and all variables are dimensional but the primes used in (1) have been dropped.

In the linearized system the baroclinic solutions are independent of M, which can be verified by defining the shear-variable $V^* \equiv V - hM/D$ or by deriving the wave equations corresponding to (6). This uncoupling of barotropic and baroclinic modes occurs here because the total transport is along the isobaths. For a complete description of the nonlinear system, an equation for the barotropic flow component may be derived. The general procedure is to eliminate the surface pressure by forming the vorticity equation for the vertically averaged flow, which in this case reduces to

$$\frac{\partial^2}{\partial t \partial x}\left(\frac{M}{D}\right) + \frac{\partial}{\partial x}\left[\frac{1}{D}\frac{\partial}{\partial x}\left(\frac{UV}{h} + \frac{UV - UM}{D-h}\right) - \frac{\tau_y}{\rho D}\right] = 0.$$

This equation shows that the shallow water near the shore will tend to move faster in the direction of the wind than the deeper water, owing to the "bottom slope vorticity" (Groen and Groves, 1962). In fact, an integration with respect to x gives

$$\frac{\partial M}{\partial t} + \frac{\partial}{\partial x}\left(\frac{UV}{h} + \frac{UV - UM}{D-h}\right) - \frac{\tau_y}{\rho} = D \times \text{constant}\,(t), \quad (9)$$

where the integration constant is actually a surface pressure gradient acting against τ_y. For the semi-infinite plane the constant may be written as $(\partial M_\infty/\partial t - \tau_y/\rho)/D_\infty$ since the nonlinear terms will vanish in open water ($x \to \infty$). This expression will be negative for any pressure gradient acting against τ_y and thus not only the mean current speed but also the integrated transport tends to be greater near the shore than in deep water. For the special case of a channel with additional boundary condition $U = 0$ for $x = L$, the integration constant can be evaluated from the mass conservation condition $\bar{M} = 0$, where the bar indicates an average over the width of the channel (Bennett, 1973). By virtue of the boundary conditions, the constant is not affected by the nonlinear terms and is equal to $\tau_y/\rho\bar{D}$. The latter will be used in the computations for Lake Ontario.

The linearized versions of Eqs. (8) reduce to the barotropic wave Eqs. (6) if only the depth is replaced by the equivalent depth $H(D-H)/D$ and the stress multiplied by $(D-H)/D$, where H is the equilibrium value of h. Within the restrictions of the linearization procedure, the lower layer depth is allowed to vary with distance from shore. The mathematical effect is that Eqs. (6) will contain coefficients which are functions of the space coordinate x. Thus the free oscillations will be solutions to the characteristic-value problem

$$g\epsilon\frac{H(D-H)}{D}\frac{\partial^2\phi}{\partial x^2} + \lambda\phi = 0, \quad \phi = 0 \text{ for } x = 0, L,$$

and the frequencies will follow from the eigenvalues λ by the relationship $\sigma_n^2 = \lambda_n + f^2$. For a given depth profile, the eigenvalues and corresponding eigenvectors are readily obtained by numerical methods. Computations for a typical Lake Ontario cross section show that the lowest few eigenvalues are up to 10% larger than those corresponding to the averaged equivalent depth, while the higher eigenvalues are smaller than their constant-depth counterparts. Thus the lower modes sense a greater-than-average equivalent depth, the higher modes feel the shallower depths. The eigenfunctions are very similar to the trigonometric functions obtained for constant depth.

The nonlinear baroclinic equations (8) also reduce to the barotropic system (2) if the upper layer is much shallower than the total depth. In that case, therefore, the results of Figs. 1–4 immediately apply to the upper layer of the present model, with the understanding that the effective acceleration of gravity is reduced by a factor ϵ and that a positive surface displacement is to be interpreted as a negative thermocline deflection. Effects of deeper upper layers may be estimated by recalling Long's (1956) solutions for large-amplitude interface perturbations in the absence of rotation or depth variations. Long (1956) considered the initial-value problem of an interface disturbance moving into a region of undisturbed shear flow. Noting that in the present case the mean transport normal to the shore

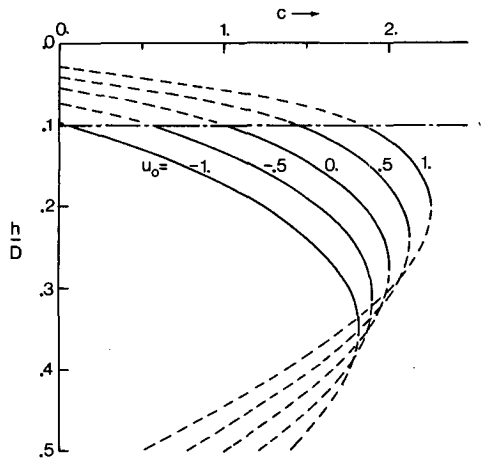

FIG. 5. Nondimensional speed of disturbance of interface depth h propagating into a region of undisturbed two-layer flow with upper layer depth equal to 0.1 D and nondimensional upper layer velocity given by u_0.

must vanish, and dividing both the upper layer fluid velocity and the wave propagation speed by the value of the internal wave speed ahead of the disturbance and in the absence of shear, the perturbation is found to move with nondimensional speed

$$c = 3(1 - 2r)[r(1 - r)]^{1/2} \frac{K}{[r_0(1 - r_0)]^{1/2}} - [1 - 6r(1 - r)] \frac{(1 - K^2)^{1/2}}{[r_0(1 - r_0)]^{1/2}},$$

where $K \equiv 2r_0u_0 + (1 - 2r_0)\{1 - [r_0/(1 - r_0)]u_0^2\}^{1/2}$, r is the ratio of upper layer depth to total depth, u the nondimensional upper layer velocity, and the subscript zero refers to the undisturbed flow.

By way of illustration, Fig. 5 shows the solution as a function of perturbation depth ratio r, for the case $r_0 = 0.1$ and u_0 ranging from -1 to 1. It is seen that the speed of propagation has a maximum in each case and thus only the portion of a wave profile corresponding to the solid lines tends to steepen. As shown by Long (1956), the maximum shifts to higher r values when r_0 is increased, but slower than r_0 itself. In particular, when the upper layer becomes deeper than the lower, the maximum wave speed for $u_0 = 0$ occurs for $r < r_0$ and hence an interface elevation tends to steepen. In that case, one would expect to see upwelling surges, but it must be recalled that the stress is multiplied by the ratio of lower layer to total depth and hence will be less effective. For the Lake Ontario simulation, the depth ratio agrees approximately with Fig. 5, and thus the conditions are favorable for the formation of depression fronts.

6. Comparison with observations

The present study was inspired by observations of temperature fronts associated with a period of strong downwelling along the south shore of Lake Ontario in August 1972. The measurements were part of the International Field Year on the Great Lakes and were concerned with the short-term behavior of internal waves (Boyce and Mortimer, 1978). Simultaneous scans of temperature-depth distributions for three cross sections of Lake Ontario were made by ships shuttling between the north and south shores for periods of 5 days. The time required to traverse each section was less than 4 h so that usually four transects were completed in one inertial period. The distance between the shores is about 70 km and the separation between adjacent transects was approximately equal to that.

By a fortunate coincidence, the most pronounced wind impulse of the 1972 summer season occurred while the transect cruises of 7–12 August were in progress. The storm and the response of the lakewide circulation and temperature distribution have been discussed in detail by Simons (1975a). The wind field was associated with an atmospheric front moving from west to east across the lake during the late afternoon of 9 August 1972. During the passage of the trough, a strong west wind built up, followed by a wind impulse from the northwest behind the front. As a result, strong downwelling was initiated along the steep south shore of the Lake. This was observed in all three cross sections with a time lag corresponding to the eastward movement of the atmospheric system of 8 ms^{-1}, i.e., ~3 h between the western and the central sections. This propagation is an order of magnitude faster than the internal wave speed in the Lake and, consequently, the thermocline response may be approximated by the rotating, one-dimensional model adopted in the previous pages. The assumptions of the model are likely best justified for the central transect which has been discussed in considerable detail by Mortimer (1977) and which is selected here for comparison with model results.

Model solutions were obtained by numerical integration of the two-layer equations (8)–(9) as applied to the central north-south cross section of Lake Ontario. The section has a length of 70 km and a maximum depth of 170 m, with a steep southern shore and a gradually sloping northern shore. Density differences across the thermocline were estimated from observed temperatures. The values were held constant in time for the whole episode, but the observed increase from less than 1×10^{-3} in deep water to about 1.5×10^{-3} near the warm downwelling shore was incorporated. The initial thermocline was taken to be horizontal ex-

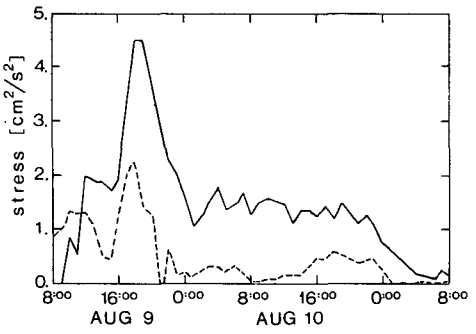

FIG. 6. Eastward (solid line) and northward (dashed line) components of wind stress derived from buoy observations in the middle of Lake Ontario for a constant drag coefficient of 1.8×10^{-3}. Stress shown includes ratio of air to water density.

cept for a region near the north shore where it was taken to slope downward in geostrophic balance with a vertical shear of the current. This was done to avoid the numerical complications of an upwelling thermocline intersecting the surface and because the earlier transects and the coastal chain data (Csanady and Pade, 1973) on 8 August indicated a deepening of the thermocline toward the north shore.

The integrations covered the period from the morning of 9 August, well before the onset of the storm, to the time of the last transect on 11 August. Wind observations were taken from the meteorological buoy network operating during the 1972 field year. Fig. 6 shows the surface stress in the middle of the Lake for a constant drag coefficient of 1.8×10^{-3}. This corresponds to typical mean values obtained for the field year by Simons (1975b) and is considerably smaller than the value required for a successful simulation of the lakewide response to this storm (Simons, 1975a). Recent measurements and simulations of wind stress in relation to surface waves by Donelan (1977) actually tend to support the larger value used before. Furthermore, Donelan's concepts lead to a steep increase of the drag coefficient while the waves are building up at the onset of the storm, and a

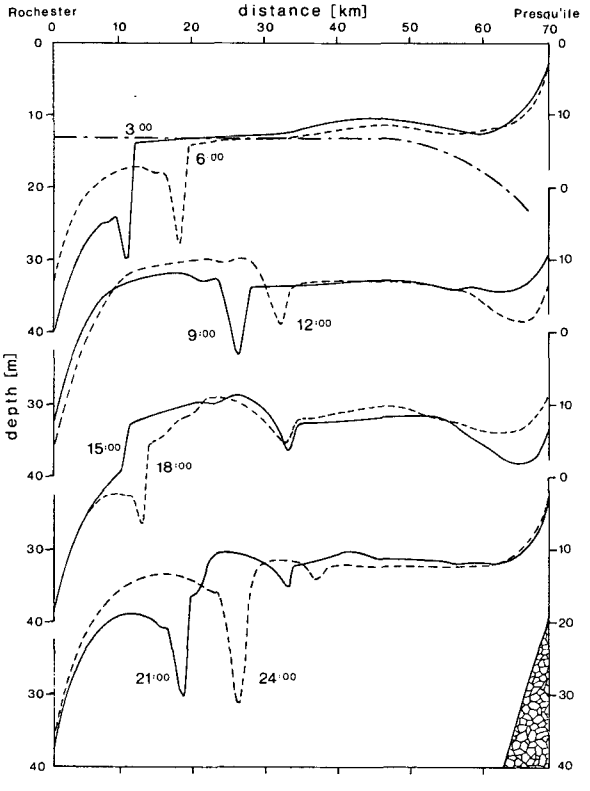

FIG. 7. Computed interface displacements in a two-layer cross-section model of Lake Ontario, after the storm of 9 August 1972 (Fig. 6). Indicated times are reckoned from 0000 GMT 10 August and refer to whole north-south thermocline profile. The alternating long and short dashes indicate initial, geostrophically balanced thermocline on the morning of 9 August.

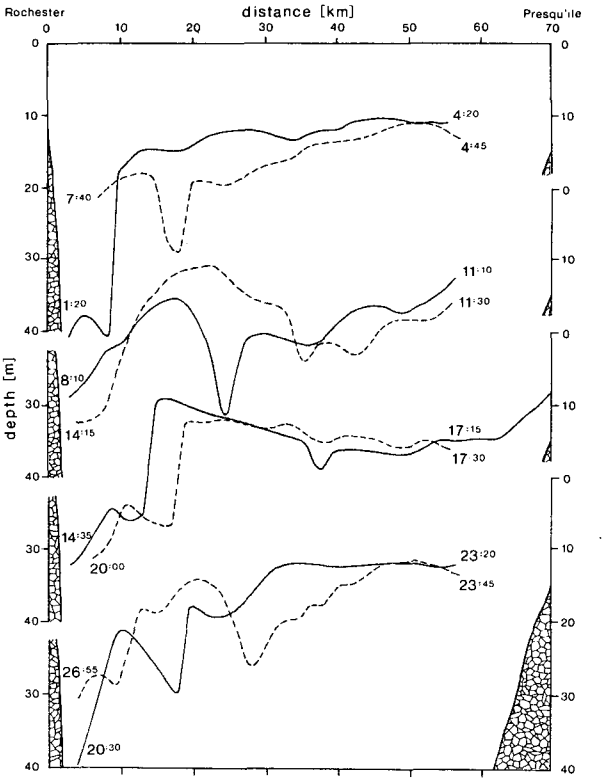

FIG. 8. Observed depths of 10°C isotherms for the same cross section and the same storm as Fig. 7. Times indicate beginning and end of repeated transects (from Boyce and Mortimer, 1976).

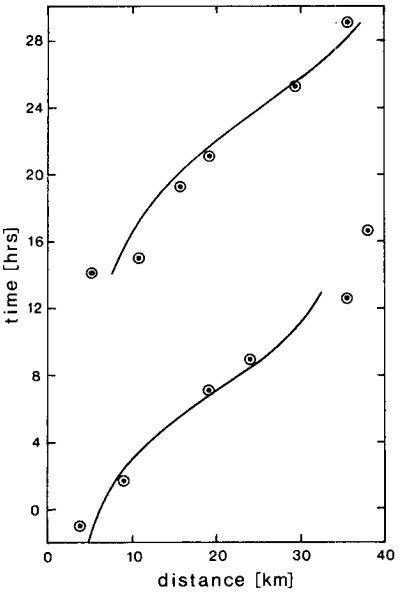

FIG. 9. Position of fronts of Figs. 7 and 8 as a function of distance from south shore and time reckoned from 0000 GMT 10 August. Curves represent computed frontal positions, circles were obtained from Mortimer (1977, Fig. 57).

drastic reduction in the stress when the wind speed drops below the phase speed of the waves after the peak of the storm. Consequently, the oscillatory response of the Lake is likely underestimated by the present simulation.

Fig. 7 presents computed thermocline configurations at intervals of 3 h for 10 August 1972. The solutions were computed with a grid spacing of 0.5 km, but calculations with larger and smaller mesh sizes gave essentially the same results. Computations with a different staggered-grid model required some smoothing by an artificial horizontal diffusion term, but again the results were basically the same. For comparison, Fig. 8 shows the depths of the 10°C isotherm as observed during the transects of 10–11 August (Boyce and Mortimer, 1978). Northward (left to right) transects are denoted by solid lines, southward transects by dashed lines, and the times of beginning and end of each transect are shown in hours and minutes. The extension of one of the isotherms into the shallow north shore region is based on simultaneous coastal chain data (Csanady and Pade, 1973). It appears that the basic kinematics of the downwelling front are simulated by the simple two-layer model.

The positions of the fronts are shown in Fig. 9 as a function of distance from the downwelling shore and time reckoned from 0000 GMT 10 August. The curves represent computed fronts while the circles have been obtained from Mortimer (1977, Fig. 57). Finally, computed upper layer currents at distances of 10 and 35 km from the downwelling shore are compared with observations in Fig. 10. The observed current for 35 km has been measured at a depth of 10 m in the present cross section of the Lake. Since no near-shore measurements are available for this cross section, the observed current for 10 km has been taken from the western cross section. This current was measured at a depth of 15 m. All times are indicated at 8 h intervals, again reckoned from 0000 GMT 10 August, for easy comparison with Figs. 7–9. In view of the time lag of the forcing between the western and central transects of the lake (~3 h), the currents at the times indicated in the lower right-hand hodograph may be expected to correspond to those accentuated in the other three hodographs. Indeed, the observed near-shore current exhibits the signature of the front about 1 h before 0000 GMT 10 August, while the computed front is seen to pass this point shortly after 0200 GMT. Like the computed current, the observed currents confirm the expected phase relationship between thermocline displacements and inertial motions. The reason that the former appear to be underestimated while the latter are overestimated in the model may be that the currents were measured relatively close to the thermocline.

7. Conclusions

This study attempted to identify the primary dynamical mechanisms responsible for the genera-

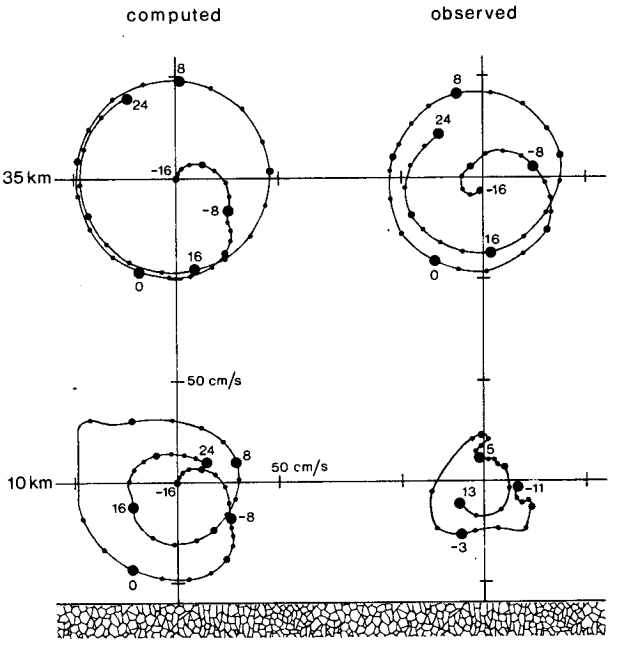

FIG. 10. Hodographs of upper layer model currents compared with measured currents at distances of 10 and 35 km from the south shore. Offshore current was observed at depth of 10 m on the same transect as Figs. 7 and 8, nearshore current at depth of 15 m on the western transect. All indicated times reckoned from 0000 GMT 10 August as in Figs. 7–9.

tion and propagation of downwelling fronts observed in Lake Ontario. Adopting the simple model of a two-layer system on a rotating, semi-infinite plane, it was recalled that under certain conditions the solutions would approach those of a single-layer model. Analytical and numerical solutions were obtained for the response of the system to a wind impulse of finite duration, and it was shown that strong nonlinear effects, in particular internal surges, could occur without invoking excessive wind speeds. A numerical simulation was carried out for actual conditions in Lake Ontario, in order to allow for a quantitative evaluation of the model.

Inasmuch as the episode simulations agree with the observations, it is concluded that the basic dynamics of the downwelling front are explained by the nonlinear wave principles considered here. The recurrence of the front after an inertial period and the proper phase relationship between thermocline deflections and inertial currents, confirm that the observed downwelling fronts are intimately connected with the oscillatory action of the inertial motion in deep water. Thus, while less detailed observations of similar temperature distributions could easily be interpreted as manifestations of baroclinic jets, the fronts are to be visualized as part of the oscillatory rather than the quasi-geostrophic response of the Lake to wind. Although disturbances from the opposite upwelling shore may eventually combine with those from the downwelling shore to create standing Poincaré waves (Mortimer, 1977), the scale of the frontal zone is sufficiently small that it can be treated independently of this effect. Thus, similar phenomena can be expected to occur in any near-shore region for suitable stratification conditions.

Acknowledgments. I would like to thank F. M. Boyce and C. H. Mortimer for many stimulating discussions and for making their interesting data sets readily available. I thank C. N. K. Mooers for suggesting many improvements in the original manuscript.

REFERENCES

Bennett, J. R., 1973: On the dynamics of wind-driven lake currents. *J. Phys. Oceanogr.*, **4**, 400–414.

Boyce, F. M., 1975: Internal waves in the Straits of Gibraltar. *Deep-Sea Res.* **22**, 597–610.

——, and C. H. Mortimer, 1978: IFYGL temperature transects. IWD Sci. Ser., Dept. of Environment, Ottawa, Canada, 363 pp. (in press).

Cahn, A., 1945: An investigation of the free oscillations of a simple current system. *J. Meteor.*, **2**, 113–119.

Carslaw, H. S., 1930: *Introduction to the Theory of Fourier's Series and Integrals*, 3rd ed. Dover, 368 pp.

Crepon, M., 1967: Hydrodynamique marine en regime impulsionnel. Part 2. *Cah. Oceanogr.*, **19**, 847–880.

Csanady, G. T., 1973: Transverse internal seiches in large oblong lakes and marginal seas. *J. Phys. Oceanogr.*, **3**, 439–447.

——, and B. Pade, 1973: The coastal jet project. Env. Fluid Mech. Lab., University of Waterloo, Ontario, Ann. Rep. 1972 to Dept. of Environment, Canada, No. OGR2-0050, 495 pp.

Donelan, M. A., 1977: A simple numerical model for wave and wind stress prediction. Canada Centre for Inland Waters, Burlington, Ontario (in preparation).

Garvine, R. W., and J. D. Monk, 1974: Frontal structure of a river plume. *J. Geophys. Res.* **79**, 2251–2259.

Groen, P., and G. W. Groves, 1962: Surges. *The Sea*, Vol. 1, M. N. Hill, Ed., Interscience, 611–647.

Houghton, D. D., 1969: Effect of rotation on the formation of hydraulic jumps. *J. Geophys. Res.* **74**, 1351–1360.

Hunkins, K., and M. Fliegel, 1973: Internal undular surges in Seneca Lake: A natural occurrence of solitons. *J. Geophys. Res.*, **78**, 539–548.

Lax, P., and B. Wendroff, 1960: System of conservation laws. *Comm. Pure Appl. Math.*, **13**, 217–237.

Long, R. R., 1956: Long waves in a two-fluid system. *J. Meteor.*, **13**, 70–74.

Mooers, C. N. K., C. A. Collins and R. L. Smith, 1976: The dynamic structure of the frontal zone in the coastal upwelling region off Oregon. *J. Phys. Oceanogr.*, **6**, 3–21.

Mortimer, C. H., 1977: Internal waves observed in Lake Ontario during the International Field Year for the Great Lakes 1972. Center for Great Lakes Studies, University of Wisconsin, Milwaukee, Spec. Rep. No. 32, 122 pp.

Rao, G. V., and T. S. Murty, 1973: Some case studies of vertical circulations associated with oceanic fronts. *J. Geophys. Res.*, **78**, 549–557.

Simons, T. J., 1975a: Verification of numerical models of Lake Ontario, Part 2: Stratified circulations and temperature changes. *J. Phys. Oceanogr.*, **5**, 98–110.

——, 1975b: Effective wind stress over the Great Lakes derived from long-term numerical model simulations. *Atmosphere*, **13**, 169–179.

Thorpe, S. A., 1971: Asymmetry of the internal seiche in Loch Ness. *Nature*, **231**, 306–308.

Winant, C. D., 1974: Internal surges in coastal waters. *J. Geophys. Res.*, **79**, 4523–4526.